Journal of Organometallic Chemistry 973–974 (2022) 122405

Contents lists available at ScienceDirect

Journal of Organometallic Chemistry

journal homepage: www.elsevier.com/locate/jorganchem

Non-peripheral tetra methoxylated pyrazoline bearing Co^{II}, Cu^{II} and $Mn^{III}Cl$ phthalocyanines: Syntheses, electrochemistry and spectroelectrochemistry

Halise Yalazan [a], Halit Kantekin [a,*], Özlem Budak [b], Atıf Koca [b]

[a] Department of Chemistry, Faculty of Sciences, Karadeniz Technical University Trabzon, Turkey
[b] Department of Chemical Engineering, Faculty of Engineering, Marmara University, Istanbul, Turkey

ARTICLE INFO

Article history:
Received 19 March 2022
Revised 14 May 2022
Accepted 26 May 2022
Available online 27 May 2022

Keywords:
Syntheses
Pyrazoline
Phthalocyanines
Electrochemistry
Spectroelectrochemistry

ABSTRACT

The novel and highly soluble cobalt(II), copper(II) and manganese(III) phthalocyanines ((***Pc*-Co, *Pc*-Cu**, and ***Pc*-Mn**) bearing 3-(5-(3,5-dimethoxyphenyl)-1-phenyl-4,5-dihydro-1*H*-pyrazol-3-yl)phenol have been synthesized and characterized by FT-IR, NMR, UV-Vis and mass spectroscopic methods. Additionally, electrochemical and spectroelectrochemical properties of these phthalocyanine compounds were investigated. Due to the redox inactivity of the Cu^{2+} central cation of (***Pc*-Cu**), Pc based reductions and oxidation processes are recorded. $[Co^{II}Pc^{2-}]/[Co^{I}Pc^{2-}]^{1-}$ and $[Co^{II}Pc^{2-}]/[Co^{III}Pc^{2-}]^{1+}$ couples for the central metal redox reactions, and $[Co^{I}Pc^{2-}]^{1-}/[Co^{I}Pc^{3-}]^{2-}$, $[Co^{I}Pc^{3-}]^{2-}/[Co^{I}Pc^{4-}]^{3-}$ and $[Co^{III}Pc^{2-}]^{1+}/[Co^{III}Pc^{1-}]^{2+}$ couples for the Pc based reduction and oxidation are observed respectively with (***Pc*-Co**). Like (***Pc*-Co**), (***Pc*-Mn**) also illustrated metal-based reduction processes, $[Cl^{1-}\text{-}Mn^{III}Pc^{2-}]/[Cl^{1-}\text{-}Mn^{II}Pc^{2-}]^{1-}$ and $[Cl^{1-}\text{-}Mn^{II}Pc^{2-}]^{1-}/[Cl^{1-}\text{-}Mn^{I}Pc^{2-}]^{2-}$ in addition to the Pc based $[Cl^{1-}\text{-}Mn^{I}Pc^{2-}]^{2-}/[Cl^{1-}\text{-}Mn^{I}Pc^{3-}]^{3-}$, $[Cl^{1-}\text{-}Mn^{I}Pc^{3-}]^{3-}$ /$[Cl^{1-}\text{-}Mn^{I}Pc^{4-}]^{4-}$ and $[Cl^{1-}\text{-}Mn^{III}Pc^{2-}]/[Cl^{1-}\text{-}Mn^{III}Pc^{1-}]^{1+}$ redox couples were also recorded. These redox mechanisms were supported with the characteristic spectral changes observed during the in-situ spectroelectrochemical measurements. Especially metal-based electron transfer changes caused distinct spectral and color changes, which are the desired properties of the complexes for the possible opto-electrochemical applications.

1. Introduction

Phthalocyanines represent an important class of macrocyclic compounds that have been used in modern applications applications, such as, cancer [1], liquid crystalline [2], electrocatalytic [3], optical and electrochemical [4], photodynamic antimicrobial activity [5], nonlinear optical [6], photodynamic therapy [7]. Due to the excellent electron transfer properties of phthalocyanines, they are also used as functional materials in various energy conversion systems [8–10]. The use of phthalocyanines in the application areas depends on the following properties: solubility, aggregation, the structure of the substituent attached to the Pc ring, the electron transfer ability, the type of metal ion in the Pc ring. Solubility properties of phthalocyanine compounds can be increased by binding bulky groups in the appropriate position in addition, phthalocyanine compounds with redox properties that are rich with suitable metal ions can be designed and their use in this field can be increased [11,12].

The most important aim of this study is to design phthalocyanine compounds that can show good solubility and electrochemical properties. Metallophthalocyanines (MPcs) are widely used in various electrochemical applications such as electrocatalytic [13–15], electrochemical sensor [16–21] and electrochromic devices [22,23] due to their superior redox activities [24–30]. The redox properties can be tailored by changing the metal center and substituent to design the required physicochemical properties [31]. MPcs containing redox active metal centers are very important in terms of their superior electroactive nature. Especially, MPcs containing Fe^{2+}, Co^{2+} and Mn^{3+} center cations have promising electrochemical properties due to their oxidation state range from M^{+} to M^{4+} [32].

In addition to the redox active metal center, the main hypothesis for choosing the pyrazoline based substituent here is that it is a bulky ligand and has intramolecular charge transfer upon excitation [33]. Pyrazolines are members of the electron-rich nitrogen-containing heterocyclic class of compounds. In recent years, it has been reported that many pyrazoline structures have a wide range of biological properties and are compounds of great interest by researchers [34].

* Corresponding author at: Department of Chemistry, Karadeniz Technical University, 61080 Trabzon, Turkey.
E-mail address: halit@ktu.edu.tr (H. Kantekin).

https://doi.org/10.1016/j.jorganchem.2022.122405
0022-328X/

As far as we know, there is one study on the electrochemical properties of phthalocyanines containing 3-(1,5-diphenyl-4,5-dihydro-1*H*-pyrazol-3-yl)phenol as the pyrazoline group, which was brought to the literature by our working group [35]. In this study, we wanted to investigate both electrochemistry and spectroelectrochemistry properties of phthalocyanines (M: Co^{II} (***Pc*-Co**), Cu^{II} (***Pc*-Cu**), $Mn^{III}Cl$ (***Pc*-Mn**)) containing methoxylated pyrazoline group and redox active/inactive metal center ions (Cu^{2+}, Co^{2+}, and Mn^{3+}). Then electrochemical and spectroelectrochemical behaviors were determined in detail in order to determine the possible usage areas of the newly synthesized MPcs. In this study, we wanted to investigate the contribution of the methoxy group to the electrochemical properties of phthalocyanine compounds. ***Pc*-Co** and ***Pc*-Mn** compounds have developed electrochemical properties by metal-based redox processes in various electrochemical application areas. Considerable color changes observed during the redox reactions indicated the solvotochromic properties of the phthalocyanines.

2. Experimental

The equipment and materials, electrochemical and *in situ* spectroelectrochemical measurements were offered as Supplementary Information.

2.1. Syntheses

2.1.1. 3-(5-(3,5-dimethoxyphenyl)-1-phenyl-4,5-dihydro-1H-pyrazol-3-yl)phenol (*Przl-OH*)

(*E*)-3-(3,5-dimethoxyphenyl)-1-(3-hydroxyphenyl)prop-2-en-1-one (**Clcn-OH**) (2g, 7.03 mmol) was solved in dry ethanol, after dissolution, phenylhydrazine (0.761g, 7.03 mmol) was added into the reaction content. Then, glacial acetic acid (1.41 mL) was attached dropwise slowly and the reaction mixture was continued with stirring at reflux temperature under N_2 atm, for 1 night. The crude product was extracted with ethyl acetate and water. Then, organic phase was evaporated and purified by column chromatography on silica gel. Consequently, title compound (**Przl-OH**) was obtained as a dark yellow oily product. The data of the **Przl-OH** compound is given below.

Yield: 94% (2.47 g).

Column chromatography solvent: ethyl acetate.

Solubility: Chloroform, ethyl acetate, ethyl alcohol, dichloromethane.

FT–IR (ATR), υ_{max} (cm^{-1}): 3305 (OH), 3060 (Ar–H), 2936–2837 (Aliph. C–H), 1654 (C=N), 1594, 1496–1455 (N–N), 1393, 1286, 1151, 1059, 998, 923, 872, 748.

^{1}H NMR (DMSO-d_6), (δ:ppm): 7.45–7.39 (m, 1H, Ar–H), 7.35–7.30 (m, 1H, Ar–H), 7.25 (d, 1H, Ar–H), 7.24 (d, 1H, Ar–H), 7.22 (d, 1H, Ar–H), 7.19 (d, 1H, Ar–H), 7.17–7.13 (m, 1H, Ar–H), 7.06–6.96 (m, 1H, Ar–H), 6.77–6.71 (m, 1H, Ar–H), 6.48–6.46 (m, 1H, Ar–H), 6.41–6.37 (m, 1H, Ar–H), 6.31 (d, 1H, Ar–H), 5.32 (t, 1H, pyrazole –CH), 5.03 (s, 1H, OH), 4.91 (dd, 1H, pyrazole $-CH_2$), 3.78 (dd, 1H, pyrazole $-CH_2$), 3.67 (s, 3H, $-OCH_3$), 3.66 (s, 3H, $-OCH_3$) .

^{13}C NMR ($CDCl_3$), (δ:ppm): 161.4, 160.9, 160.5, 151.8, 146.9, 146.5, 143.45, 140.8, 133.9, 133.8, 132.6, 131.7, 128.9, 127.9, 125.6, 122.4, 119.8, 119.3, 100.8, 55.4 (OCH_3), 55.3 (OCH_3), 55.3 (pyrazole –CH), 43.5 (pyrazole $-CH_2$).

MALDI–TOF–MS *m*/z: Calculated for $C_{23}H_{22}N_2O_3$: 374.43; Found: 374.71 $[M]^+$.

2.1.2. 3-(3-(5-(3,5-dimethoxyphenyl)-1-phenyl-4,5-dihydro-1H-pyrazol-3-yl)phenoxy) phthalonitrile (*Przl-CN*)

3-(5-(3,5-dimethoxyphenyl)-1-phenyl-4,5-dihydro-1*H*-pyrazol-3-yl)phenol (**Przl-OH**) (1.12g, 2.99 mmol) was solved in dry DMF, after dissolution, 3-nitrophthalonitrile (0.52g, 2.99 mmol) was added into the reaction content. Then, anhydrous potassium carbonate (1.24g, 8.97 mmol) was added and the reaction mixture was continued with stirring at 60 °C under N_2 atm, for 113 hours. The crude product was poured onto ice, filtered, purified by column chromatography upon aluminum oxide. Consequently, title compound (**Przl-CN**) was obtained as a yellow colored solid product. The data of the phthalonitrile compound (**Przl-CN**) is given below.

Yield: 52% (0.78 g).

Melting point: 88−90 °C.

Column chromatography solvent: Ethyl acetate

Solubility: Chloroform, ethyl acetate, ethyl alcohol, dichloromethane

FT–IR (ATR), υ_{max} (cm^{-1}): 3079 (Ar–H), 2936–2837 (Aliph. C–H), 2231 (C≡N), 1659 (C=N), 1594, 1455−1428 (N–N), 1385, 1354, 1267, 1203–1153–1059 (Ar–O–Ar), 991, 927, 836, 792, 749.

^{1}H NMR ($CDCl_3$), (δ:ppm): 7.83 (d, 1H, Ar–H), 7.73 (d, 1H, Ar–H), 7.70–7.68 (m, 1H, Ar–H), 7.65–7.63 (m, 1H, Ar–H), 7.59–7.51 (m, 1H, Ar–H), 7.49–7.43 (m, 1H, Ar–H), 7.38–7.32 (m, 1H, Ar–H), 7.21–7.01 (m, 1H, Ar–H), 6.94–6.91 (m, 1H, Ar–H), 6.87–6.83 (m, 1H, Ar–H), 6.82 (s, 1H, Ar–H), 6.55 (d, 1H, Ar–H), 6.46 (d, 1H, Ar–H), 6.42 (d, 1H, Ar–H), 6.38–6.34 (m, 1H, Ar–H), 5.20 (t, 1H, pyrazole –CH), 5.07 (dd, 1H, pyrazole $-CH_2$), 3.83 (dd, 1H, pyrazole $-CH_2$), 3.74 (s, 3H, $-OCH_3$), 3.73 (s, 3H, $-OCH_3$).

^{13}C NMR ($CDCl_3$), (δ:ppm): 161.6, 161.4, 160.9, 160.6, 154.1, 154.0, 150.4, 145.3, 145.1, 144.7, 144.6, 144.4, 134.4, 134.3, 131.7, 130.7, 129.1, 128.9, 128.8, 127.8, 126.8, 125.3, 123.5, 117.3 (C≡N), 117.2 (C≡N), 113.5, 106.8, 55.4 (OCH_3), 55.3 (OCH_3), 55.3 (pyrazole –CH), 43.2 (pyrazole $-CH_2$).

MALDI–TOF–MS *m*/z: Calculated for $C_{31}H_{24}N_4O_3$: 500.55; Found: 500.84 $[M]^+$.

2.1.3. General syntheses of Co^{II}, Cu^{II} and $Mn^{III}Cl$ phthalocyanines bearing methoxylated pyrazoline (*Pc-Co, Pc-Cu and Pc-Mn*)

Phthalonitrile compound (**Przl-CN**) (0.1 g, 0.199 mmol for ***Pc*-Co**, ***Pc*-Cu** *and* ***Pc*-Mn**) was solved in 1-pentanol (4 mL), after dissolution, related anyhdrous metal salt $CoCl_2$ or $CuCl_2$ (13 mg, 0.099 mmol for the compounds ***Pc*-Co** and ***Pc*-Cu**) or $MnCl_2$ (12 mg, 0.099 mmol for the compound ***Pc*-Mn**) was added into the reaction content. Then, DBU (5 drops) was added dropwise slowly and the reaction mixture was continued with stirring at reflux temperature under N_2 atm, for 19 hours. The crude product was precipitated with ethanol, filtered and purified by column chromatography upon aluminium oxide. Consequently, Co^{II} (***Pc*-Co**) and Cu^{II} (***Pc*-Cu**) phthalocyanines were obtained as turquoise blue solids, and manganese phthalocyanine (***Pc*-Mn**) was acquired as brown solid. The data of the Co^{II}, Cu^{II} and $Mn^{III}Cl$ phthalocyanines are given below.

2.1.3.1. 3-(3-(5-(3,5-dimethoxyphenyl)-1-phenyl-4,5-dihydro-1H-pyrazol-3-yl)phenoxy) phthalocyaninato cobalt(II)(**Pc-Co**). Yield: 24% (24 mg), m.p. >300 °C.

Solvent system of column chromatography: C_2H_5OH:$CHCl_3$ (0.05:5 v/v)

FT–IR (ATR), υ_{max} (cm^{-1}): 3058 (Ar–H), 2999–2928−2836 (Aliph. C–H), 1591, 1456, 1353, 1243, 1152, 1059, 991, 836, 747.

UV–Vis ($CHCl_3$), λ_{max}, nm (logε): 689 (5.07), 622 (4.53), 335 (4.92).

MALDI–TOF–MS *m/z*: Calculated for $C_{124}H_{96}N_{16}O_{12}Co$: 2061.12; Found: 2061.16 $[M]^+$.

2.1.3.2. 3-(3-(5-(3,5-dimethoxyphenyl)-1-phenyl-4,5-dihydro-1H-pyrazol-3yl)phenoxy) phthalocyaninato copper(II) (Pc-Cu). Yield: 34% (35 mg), m.p. >300 °C.

Solvent system of column chromatography: C_2H_5OH:$CHCl_3$ (0.05:5 v/v)

FT–IR (ATR), υ_{max} (cm^{-1}): 3058 (Ar–H), 2953–2918–2849 (Aliph. C–H), 1591, 1456, 1353, 1203, 1152, 1058, 991, 835, 744.

UV–Vis ($CHCl_3$), λ_{max}, nm (logε): 701 (5.16), 630 (4.53), 330 (4.75).

MALDI–TOF–MS *m/z*: Calculated for $C_{124}H_{96}N_{16}O_{12}Cu$: 2065.74; Found: 2065.35 $[M]^+$.

2.1.3.3. 3-(3-(5-(3,5-dimethoxyphenyl)-1-phenyl-4,5-dihydro-1H-pyrazol-3yl)phenoxy) phthalocyaninato manganese(III)chloride (**Pc-Mn**). Yield: 27% (28 mg), m.p. >300 °C.

Solvent system of column chromatography: C_2H_5OH:$CHCl_3$ (0.05:5 v/v)

FT–IR (ATR), υ_{max} (cm^{-1}): 3063 (Ar–H), 2997–2932–2836 (Aliph. C–H), 1591, 1496, 1455, 1323, 1243, 1151, 1059, 991, 895, 742.

UV–Vis ($CHCl_3$), λ_{max}, nm (logε): 757 (5.06), 694 (4.49), 536 (4.33), 354 (4.87).

MALDI–TOF–MS *m/z*: Calculated for $C_{124}H_{96}N_{16}O_{12}MnCl$:2092.58; Found:2093.76 $[M+H]^+$.

3. Results and discussion

3.1. Characterization of synthesized compounds

The general synthesis scheme of methoxylated pyrazoline (**Pyrzl-OH**), its phthalonitrile derivative (**Pyrzl-CN**) and methoxylated pyrazoline bearing Co^{II} (***Pc*-Co**), Cu^{II} (***Pc*-Cu**) and $Mn^{III}Cl$ (***Pc*-Mn**) phthalocyanines is given in Scheme 1.

The structure of the novel metoxylated pyrazoline (**Pyrzl-OH**) was characterized using MALDI-TOF mass, FT-IR, ^{13}C NMR and ^1H NMR spectral data. The IR spectrum of the pyrazolines disclosed absorption bands in the regions 1654 cm^{-1} corresponding to the C=N stretching bands on account of ring closure. Furthermore, the absorption bands (N–N) at 1496–1455 cm^{-1} revealed stretching vibrations, proving the formation of the pyrazoline ring (Fig.S1). The ^1H NMR and ^{13}C NMR spectra of the metoxylated pyrazoline (**Pyrzl-OH**) were taken in $CDCl_3$. The obtained pyrazoline compound has characteristic peaks known as doublet of doublet (dd) in the ^1H NMR spectrum and these peaks were observed at 4.91 and 3.72 ppm. The aromatic ring protons of this compound were seen among 7.45–6.31 ppm (Fig.S6). In the ^{13}C-NMR spectrum, the carbon atom resonances of the pyrazoline compound were seen at 43.5, 55.3 and 151.8 ppm and these signals prove the formation of the newly formed pyrazoline ring (Fig.S7). The mass spectrum of pyrazoline derivative, the molecular ion peak was observed at m/z: 374.71 $[M]^+$ (see Fig. 1).

The phthalonitrile derivative (**Pyrzl-CN**) was characterized by the same spectroscopic methods as the metoxylated pyrazoline compound. Looking at the FT-IR spectrum of the phthalonitrile compound (**Pyrzl-CN**), the –OH stretching vibration of the pyrazoline compound (**Pyrzl-OH**) at 3305 cm^{-1} disappeared and showed the typical C≡N stretching vibration at 2231 cm^{-1} (Fig. S2). ^1H / ^{13}C NMR spectra of the phthalonitrile derivative were taken in $CDCl_3$. In the ^1H NMR spectrum of phthalonitrile compound (**Pyrzl-CN**), the aromatic protons were seen between 7.82–6.34 ppm. The pyrazole –CH protons were observed at 5.20 ppm, also the pyrazole $–CH_2$ proton was seen at 5.07 and 3.83 ppm (Fig. S8). When the ^{13}C NMR spectrum was examined, the nitrile carbon atoms of the phthalonitrile compound (**Pyrzl-CN**) were observed at 117.3 and 117.2 ppm. In addition, the carbon atom of pyrazole ring (pyrazole –C=N), the carbon atom of pyrazole ring (pyrazole –CH) and the carbon atom of pyrazole ring (pyrazole $–CH_2$) were seen at 150.4, 55.3 and 43.2 ppm, respectively (Fig. S9). The mass spectrum of pyrazoline substituted phthalonitrile (**Pyrzl-CN**), the molecular ion peak was seen at m/z: 500.84 $[M]^+$ (see Fig. 1).

When the FT-IR spectra was examined of Co^{II}, Cu^{II} and $Mn^{III}Cl$ phthalocyanines, the typical C≡N stretching vibration of the phthalonitrile was not observed (Fig. S3–S5). In addition to the structural characterization of pyrazoline and phthalonitrile compounds, UV-Vis spectrum was used for the structural elucidation of phthalocyanine compounds. In the UV-Vis spectrum, which is one of the most important indicators of the formation of phthalocyanine compounds, Pcs have two absorption bands known as Q and B bands. The UV–Vis spectra of Co^{II} (***Pc*-Co**), Cu^{II} (***Pc*-Cu**) and $Mn^{III}Cl$ (***Pc*-Mn**) phthalocyanines compounds were taken in $CHCl_3$ at a concentration of 1.0×10^{-5} M. The Q bands of these compounds were observed at approximately 757–689 nm and the B bands about 354–330 nm (see Fig. 2). Besides, ***Pc*-Mn** exhibited the new absorption band at around 536 nm in addition to the B band. Because $MnCl_2$ was used in the synthesis of the Pcs, the formation of $Mn^{II}Pc$ was expected. However, Q band absorption in the UV–Vis spectrum of the $Mn^{II}Pc$ (***Pc*-Mn**) is redshifted. This observation recommended the formation of the $Mn^{III}Cl$ type phthalocyanine. The aerobic conditions in purification processes were presumably the main reason for the formation of $Mn^{III}ClPc$ product [36]. The UV–Vis spectrum of ***Pc*-Mn** is openly distinct from the spectrum of the ***Pc*-Co** and ***Pc*-Cu**. The oxidation state of Mn in the complex with Pc is +3, while the other metal Co and Cu are in oxidation state +2. The Q band of ***Pc*-Mn** is shifted by 50–70 nm compared the Q band of the other ***Pc*-Co** and ***Pc*-Cu**. Also, the UV–Vis spectrum of ***Pc*-Mn** is typical of $Mn^{III}ClPc$ with a red shifted Q band at 757 nm. The red shift is a result of lowering of HOMO-LUMO gap, by either the destabilizing of the HOMO or stabilizing of the LUMO by the central metal [37,38]. When we look at the literature, MnPc phthalocyanines with different substituents show similar absorption properties [12,13,39,40]. When the mass spectra of phthalocyanines were analyzed, the molecular ion peaks were exhibited at m/z values of 2061.16 $[M]^+$ (***Pc*-Co**), 2065.35 $[M]^+$ (***Pc*-Cu**) and 2093.76 $[M+H]^+$ (***Pc*-Mn**) (see Fig. 3).

The data obtained show that the structures of all the compounds were formed and the obtained data were also compatible with the anticipated structures as stated in Section 2.

3.2. Voltammetric measurements

It is well documented that the redox functionalities are related with Pc ring, metal center and substituent based electron transfer reactions [41–46]. While Pc ring can undergo up to four reduction and two oxidation reactions depending on the electrolyte potential windows. However, it is not always possible to record all these processes due to the narrow potential window of the electrolytes. At least two reduction and two oxidation processes could be recorded in the DMSO and DCM electrolytes. In addition to the Pc based processes, redox active metal centers can illustrate addition redox processes before the Pc based ones. The position and character of the redox processes of Pc and metal centers can be altered by the electron donating or withdrawing ability of the substituents. Substituents may also give redox processes and significantly influence aggregation tendencies and solubility of the complexes [45,46]. Here MPcs bearing 3-(5-(3,5-dimethoxyphenyl)-1-phenyl-4,5-dihydro-1*H*-pyrazol-3-yl)phenol substituents supply solubility of the complexes in DCM/TBAP electrolyte. Thus, redox reactions of all complexes could be carried out in 5.0 10^{-5} mol dm^{-3} concentration in this electrolyte and half wave potentials of the redox couples derived from the voltammograms are tabulated in Table 1. As shown in Fig. 4 and Table 1, ***Pc*-Cu** illustrated four reduction and one oxidation reaction within the potential windows of the electrolyte. All of these processes can be easily attributed to the Pc ring due to the redox inactivity of the Cu^{2+} cation in the core of the Pc ring. Due to the aggregation of the complex especially reduction processes get complicated with the electron transfer re-

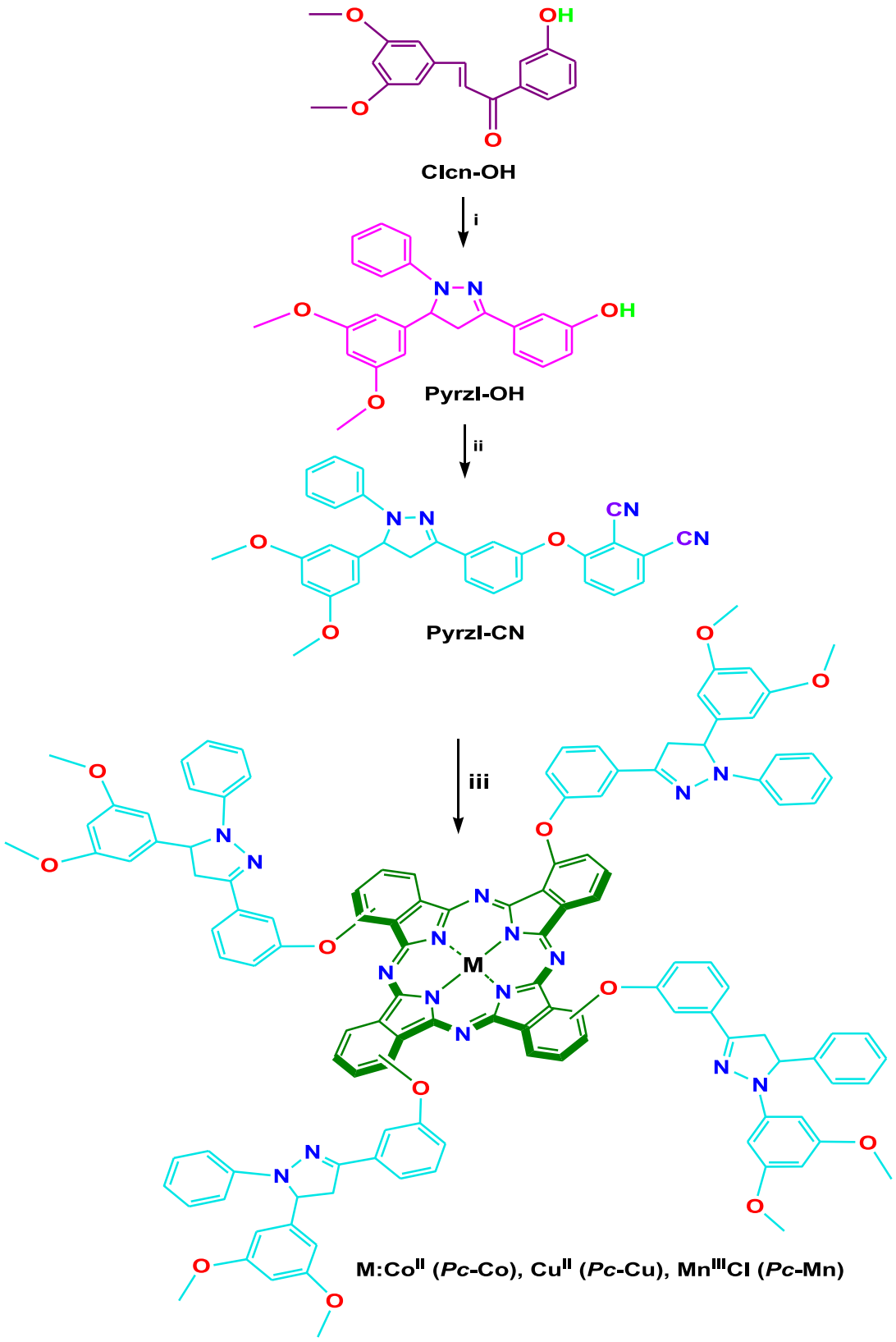

Scheme 1. Synthesis scheme of all synthesized compounds (**PrzI-OH, PrzI-CN, *Pc*-Co, *Pc*-Cu** and ***Pc*-Mn**). Reagents and conditions (i) ethanol, phenylhydrazine, glacial acetic acid, reflux temperature (ii) N_2, K_2CO_3, DMF, 60 ^{0}C (iii) N_2, 1-pentanol, DBU, $CoCl_2$, $CuCl_2$, $MnCl_2$, reflux temperature.

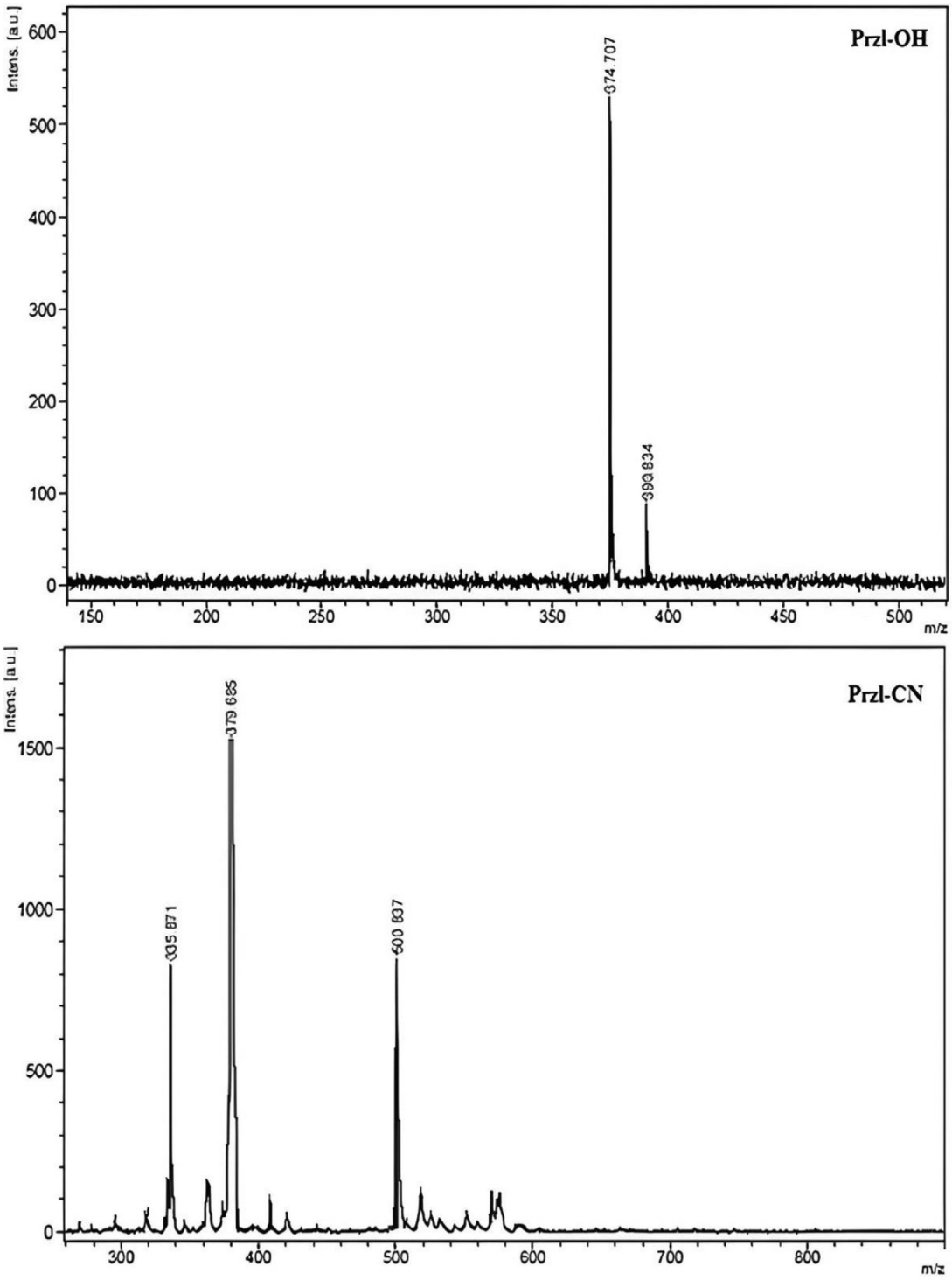

Fig. 1. Mass spectra of pyrazoline and phthalonitrile compounds (**Przl-OH** and **Przl-CN**).

actions of aggregated and non-aggregated species at similar potentials. Due to this issue redox couples are split into two waves. CVs recorded with different vertex potentials clearly illustrate the influence of the aggregation to the redox behaviors of the complex. Electron releasing nature of 3-(5-(3,5-dimethoxyphenyl)-1-phenyl-4,5-dihydro-1*H*-pyrazol-3-yl)phenol substituents cause to shifting of the redox coupes towards the negative potentials with respect to similar complexes in the literature as shown in Table 1 [31].

Changing of the metal center of Pc from Cu^{2+} to Co^{2+} significantly influenced the redox response of the complex. As shown in Fig. 5, three reduction and two oxidation processes are observed with the CVs and SWVs of Pc-Co. Observation of the R(1) at -0.43 V and Ox(1) at 0.18 V at the potentials very close to 0 V are completely different than the Pc based processes. Since Pc bassed reduction and oxidation processes can be generally observed after -0.60 V and 0.70 V respectively. When compared with the similar CoPcs given in Table 1, the Red (1) and Ox(1) couples are easily assigned to $[Co^{II}Pc^{2-}]/[Co^{I}Pc^{2-}]^{1-}$ and $[Co^{II}Pc^{2-}]/[Co^{III}Pc^{2-}]^{1+}$ processes. After the R(1) couple, Pc based R(2) at -1.38 V, and R(3) at -1.96 V are olso observed during the cathodic potential scans. More-

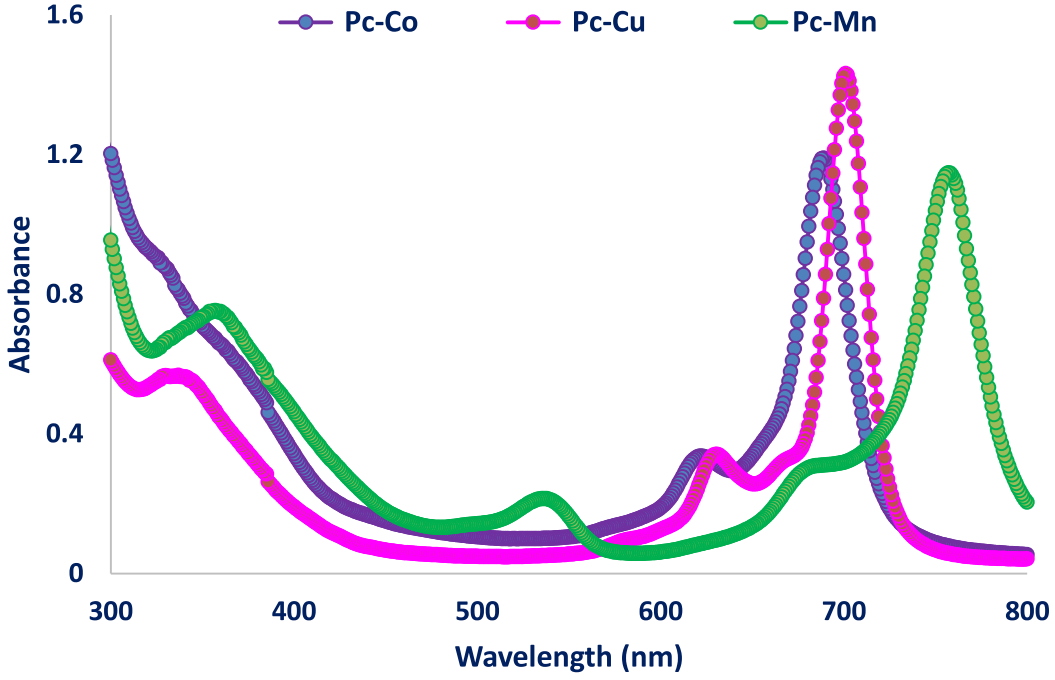

Fig. 2. UV-Vis spectra of Co^{II}, Cu^{II} and $Mn^{III}Cl$ phthalocyanines (***Pc*-Co, *Pc*-Cu** and ***Pc*-Mn**) in $CHCl_3$ (C:1 × 10^{-5}M).

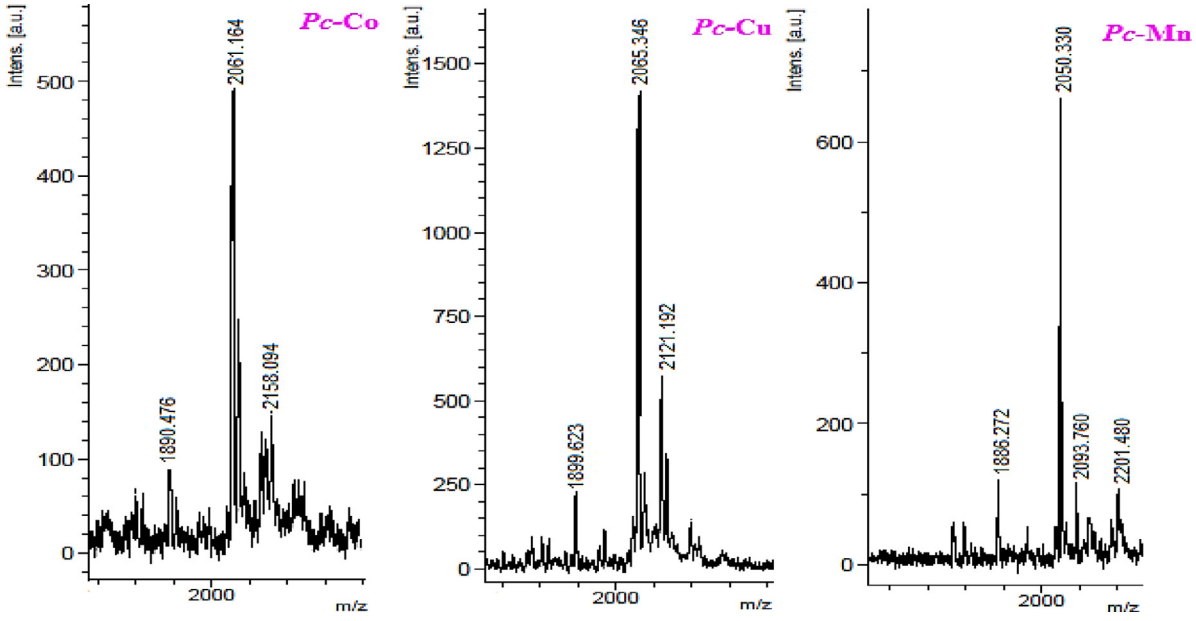

Fig. 3. Mass spectra of Co^{II}, Cu^{II} and $Mn^{III}Cl$ phthalocyanines (***Pc*-Co, *Pc*-Cu** and ***Pc*-Mn**).

over, after the and $[Co^{II}Pc^{2-}]/[Co^{III}Pc^{2-}]^{1+}$ process, the second oxidation couple Ox(2) assigned to the Pc based process is observed at 0.97 V. With respect to these assignments the mechanism given in Scheme 2 is proposed. This mechanism was also suprroted with the in situ spectroelectrochemical measurements discussed below. Similar voltammetric mechanisms (metal-Pc-Pc based reductions and metal-Pc based oxidations) were reported with Nyokong et al. [17,41,44]. In a review article, Koca A. summurized the electrochemistry of MPcs and reported the same mechanism for CoPcs in polar electrolyte [45]. With respect to peak to peak separation (ΔE_p), and peak current ratio (I_{pa}/I_{pc}), while the R(1), R(2), and Ox(1) are electrochemically and chemically reversible, the other processes are chemically quasi-reversible. Reversibility of the processes are supported with the CVs recorded with various vertex potentials (Fig. 5b). These analyses are also supported with the ca. unity of the I_{pa}/I_{pc} ratios of R(1), R(2), and Ox(1) couples shown in SWVs (Fig. 5b).

$$\left[Co^{III}Pc^{2-}\right]^{1+} - e^{-} \overset{E_{1/2}=0.97\ V\ (O(2))}{\Longleftrightarrow} \left[Co^{III}Pc^{1-}\right]^{2+}$$

$$\left[Co^{II}Pc^{2-}\right] - e^{-} \overset{E_{1/2}=0.18\ V\ (O(1))}{\Longleftrightarrow} \left[Co^{III}Pc^{2-}\right]^{1+}$$

$$\left[Co^{II}Pc^{2-}\right] + e^{-} \overset{E_{1/2}=-0.43\ V\ (R(1))}{\Longleftrightarrow} \left[Co^{I}Pc^{2-}\right]^{1-}$$

$$\left[Co^{I}Pc^{2-}\right]^{1-} + e^{-} \overset{E_{1/2}=-1.38\ V\ (R(2))}{\Longleftrightarrow} \left[Co^{I}Pc^{3-}\right]^{2-}$$

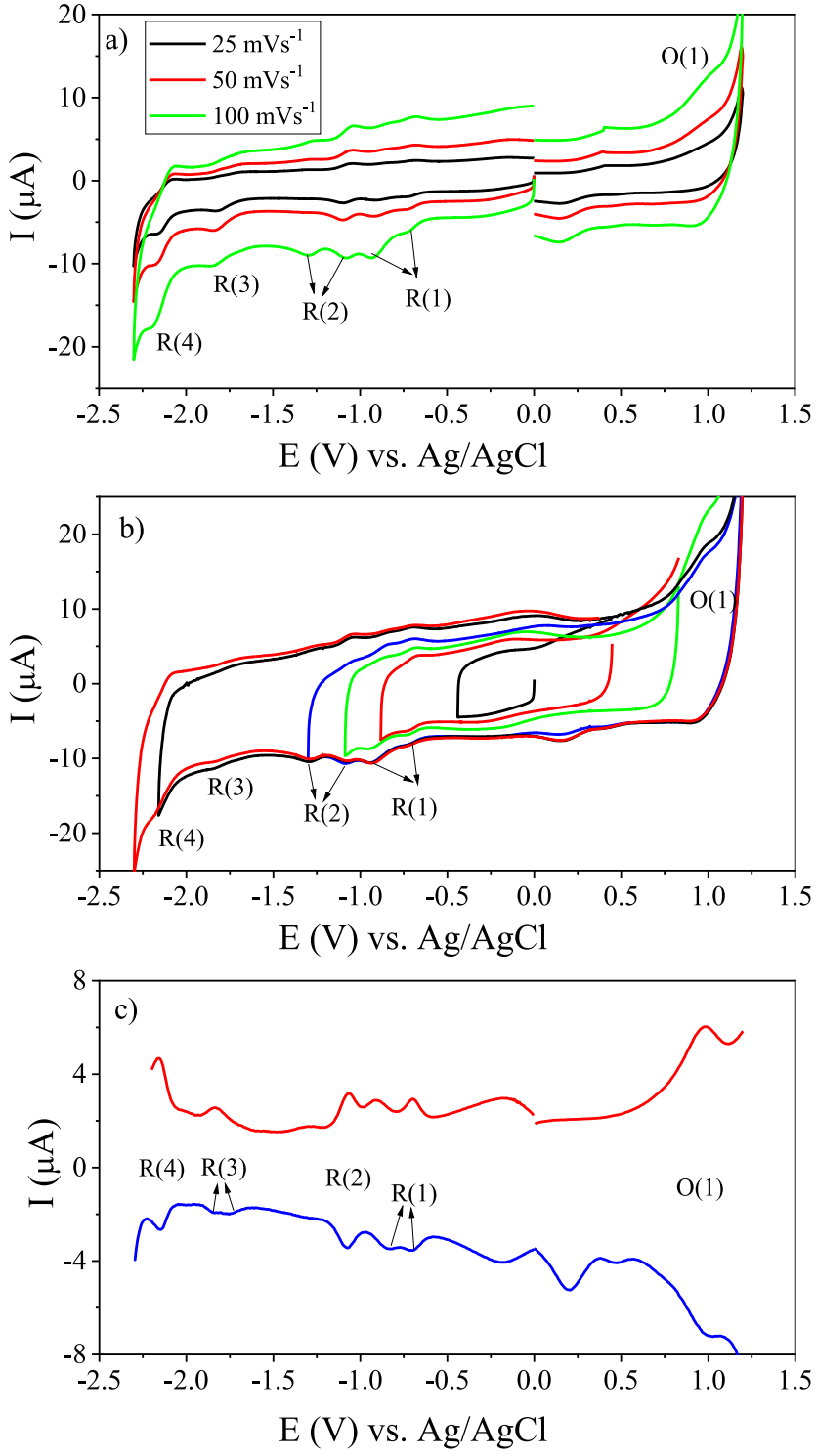

Fig. 4. CVs and SWVs of ***Pc*-Cu** (5.0×10^{-4} mol.dm^{-3}) recorded at various scan rates on a GCE working electrode in DMSO/TBAP.

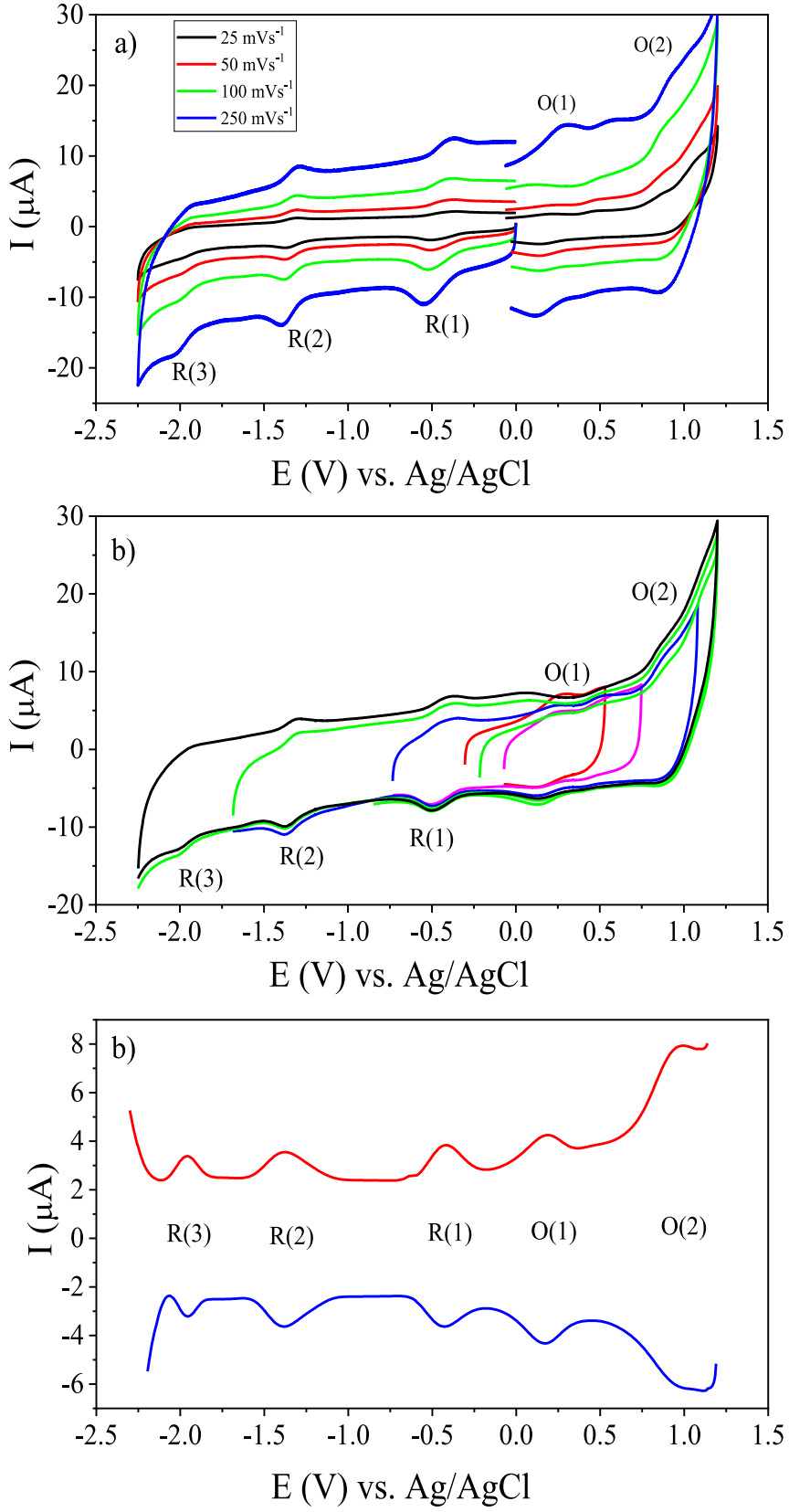

Fig. 5. CVs and SWVs of ***Pc*-Co** (5.0×10^{-4} mol.dm^{-3}) recorded at various scan rates on a GCE working electrode in DMSO/TBAP.

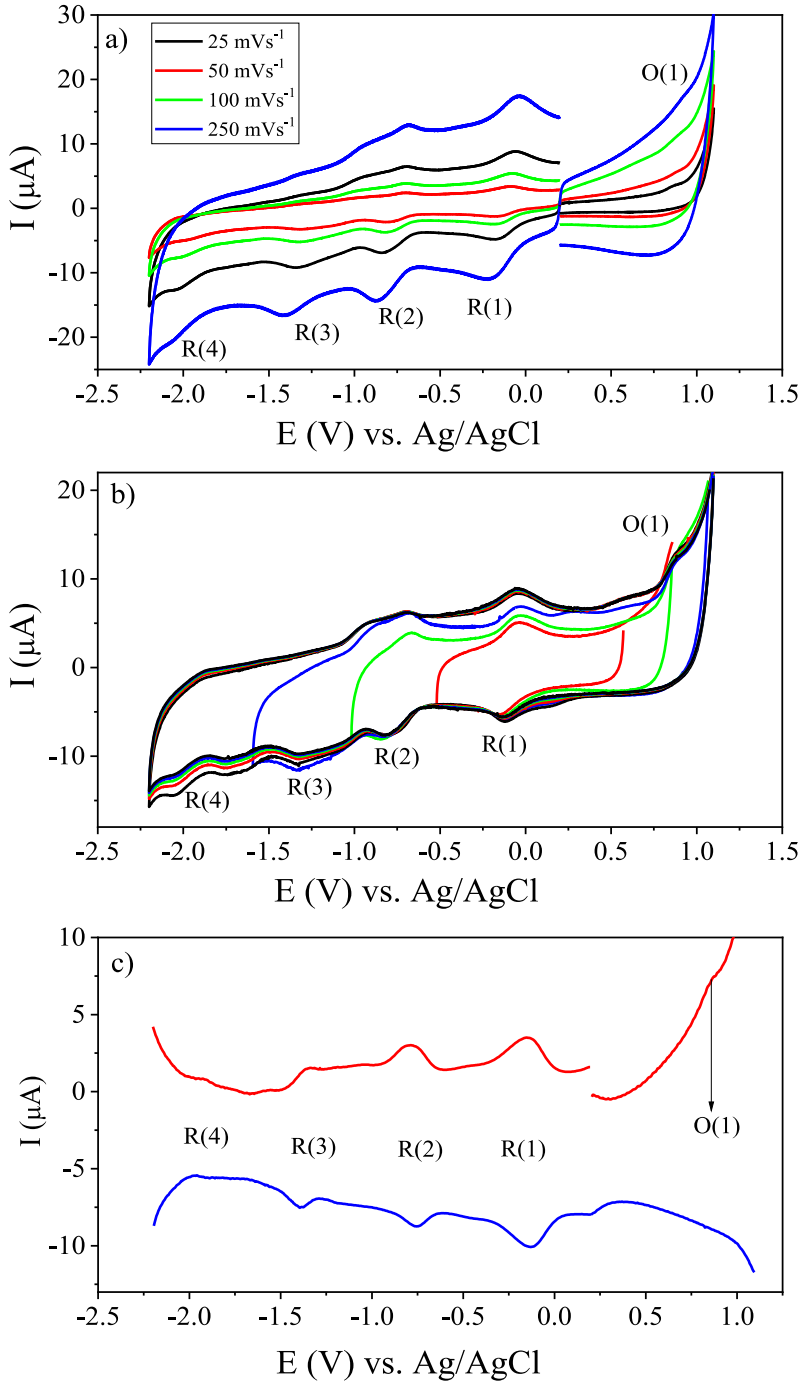

Fig. 6. CVs and SWVs of ***Pc*-Mn** (5.0×10^{-4} mol.dm^{-3}) recorded at various scan rates on a GCE working electrode in DMSO/TBAP.

Table 1
Electrochemical data of the complexes in DMSO/TBAP solution. All potentials were given versus Ag/AgCl.

	$E_{1/2}$ (V) of Redox Processes						
Complexes	Red.(I)	Red.(II)	Red.(III)	Red.(IV)	Oxd.(I)	Oxd.(II)	Ref.
CuPc (*Pc*-Cu)	-0.70 (-0.84)	-1.07 (-1.30)	-1.83	-2.15	0.98	-	tw
CoPc (*Pc*-Co)	-0.43	-1.38	-1.96		0.18	0.97	tw
MnClPc (*Pc*-Mn)	-0.13	-0.75	-1.38	-1.91	0.86	-	tw
CoPc	-0.48	-1.29	-1.92		0.30	0.91	[60]
CoPc	-0.38	-1.30	-		0.39	-	[61]
CoTMPyrPc	-0.50	-1.34	-1.93		0.47	1.00	[62]
CoTMPyrPc	-0.26	-1.25	-1.84		0.52	1.00	[52]
CuPc(mpt)	-0.95	-1.21	-1.88		0.58	1.30	[53]
CuPc	-0.70	-1.02	-		0.68	1.13	[52]
CuPc	-0.73	-1.08	-1.64		-	-	[61]
MnClPc	-0.30	-0.90	-1.36		0.38 (0.51)	0.88	[60]
MnClPc	-0.08	-0.84	-		0.30	0.87	[50]
MnTMPyrPc	-0.06	-0.68	-1.19		-	-	[62]
MnClPc(m)	-0.23	-0.80	-1.04		-	-	[63]

[a] The potentials given in parantehesis are assigned to the electron transfer reactions of the aggregated species.
[b] The potentials given in parantehesis are assigned to the electron transfer reactions of the species produced with chemical reactions (See scheme 3).

$$[Co^{III}Pc^{2-}]^{1+} - e^- \overset{E_{1/2}=0.97\ V\ (O(2))}{\Longleftrightarrow} [Co^{III}Pc^{1-}]^{2+}$$

$$[Co^{II}Pc^{2-}] - e^- \overset{E_{1/2}=0.18\ V\ (O(1))}{\Longleftrightarrow} [Co^{III}Pc^{2-}]^{1+}$$

$$[Co^{II}Pc^{2-}] + e^- \overset{E_{1/2}=-0.43\ V\ (R(1))}{\Longleftrightarrow} [Co^{I}Pc^{2-}]^{1-}$$

$$[Co^{I}Pc^{2-}]^{1-} + e^- \overset{E_{1/2}=-1.38\ V\ (R(2))}{\Longleftrightarrow} [Co^{I}Pc^{3-}]^{2-}$$

$$[Co^{I}Pc^{3-}]^{2-} + e^- \overset{E_{1/2}=-1.96\ V\ (R(3))}{\Longleftrightarrow} [Co^{I}Pc^{4-}]^{3-}$$

Scheme 2. Redox mechanism of ***Pc*-Co**.

$$\left[Co^{I}Pc^{3-}\right]^{2-} + e^- \overset{E_{1/2}=-1.96\ V\ (R(3))}{\Longleftrightarrow} \left[Co^{I}Pc^{4-}\right]^{3-}$$

Like ***Pc*-Co, *Pc*-Mn** has also redox active metal center [47,48]. Thus, it illustrates metal based reduction processes in addition to the Pc based electron transfer reactions. When compared with the similar MnPcs reported in the literature, R(1) at-0.13 V and R(2) at-0.75 V are assigned to the Mn^{3+}/Mn^{2+} and Mn^{2+}/Mn^{+} reductions respectively (Fig. 6) [42,47,49,50]. Moreover, Pc based processes are also observed at -1.38 V (R(3)), -1.91V (R(4)), and 0.86 V (Ox1)). This proposed mechanism is represented in Scheme 3. The proposed mechanism was supported with the in-situ spectroelectrochemical measurements discussed below. Due to the releasing of the axial Cl^{-1} ligand after the R(2) process, further redox processes are complicated with the following chemical reactions as shown in Fig. 6b and c. Due to the chemical reactions, especially R(3) and R(4) couples get chemically irreversible and small waves are observed after and before the R(3) at around -1.11 V and -1.63 V.

$$\left[Cl^{1-} - Mn^{III}Pc^{2-}\right] - e^- \overset{E_{1/2}=0.86\ V\ (O(1))}{\Longleftrightarrow} \left[Cl^{1-} - Mn^{II}Pc^{1-}\right]^{1+}$$

$$\left[Cl^{1-} - Mn^{III}Pc^{2-}\right] + e^- \overset{E_{1/2}=-0.13\ V\ (R(1))}{\Longleftrightarrow} \left[Cl^{1-} - Mn^{II}Pc^{2-}\right]^{1-}$$

$$\left[Cl^{1-} - Mn^{II}Pc^{2-}\right]^{1-} + e^- \overset{E_{1/2}=-0.75\ V\ (R(2))}{\Longleftrightarrow} \left[Cl^{1-} - Mn^{I}Pc^{2-}\right]^{2-}$$

$$\left[Cl^{1-} - Mn^{I}Pc^{2-}\right]^{2-} \leftrightarrow \left[Mn^{I}Pc^{2-}\right]^{1-} + Cl^{1-}$$

$$\left[Mn^{I}Pc^{2-}\right]^{1-} + e^- \overset{E_{1/2}=-1.11\ V}{\Longleftrightarrow} \left[Mn^{I}Pc^{3-}\right]^{2-}$$

$$\left[Cl^{1-} - Mn^{I}Pc^{2-}\right]^{2-} + e^- \overset{E_{1/2}=-1.38\ V\ (R(3))}{\Longleftrightarrow} \left[Cl^{1-}Mn^{I}Pc^{3-}\right]^{3-}$$

$$\left[Mn^{I}Pc^{3-}\right]^{2-} + e^- \overset{E_{1/2}=-1.63\ V}{\Longleftrightarrow} \left[Mn^{I}Pc^{4-}\right]^{3-}$$

$$\left[Cl^{1-}Mn^{I}Pc^{3-}\right]^{3-} + e^- \overset{E_{1/2}=-1.91\ V\ (R(4))}{\Longleftrightarrow} \left[Cl^{1-}Mn^{I}Pc^{4-}\right]^{4-}$$

3.3. In-Situ Spectroelectrochemical measurements

Electrochemical derived from the voltametric analyses are realized with in-situ spectroelectrochemical measurements (SEC). Additionally, color and spectra of the different oxidation states of the complexes are determined with these measurements. Fig. 7 illustrates spectral and color changes recorded during the redox reactions of ***Pc*-Cu**. As shown in Fig. 7a-c, changing the intensity of the Q band without a shift and observation of new bands due to the ligand to metal charge transfer processes supported the Pc ring based electron transfer reactions [46,51,52]. Neutral CuPc gives the Q band at 695 nm and the B band at 378 nm. Under -1.0 V applied potential the Q band decrease in absorption intensity without a shift and two new bands are enhanced at 598 and 790 nm, due to the $[Cu^{II}Pc^{2-}]$ / $[Cu^{II}Pc^{3-}]^{1-}$reduction. Clear isosbestic points at 370, 610, and 740 nm, indicating chemical reversibility of the reduced species (Fig. 7a) [53,54]. During the R(2) process, while the Q band is completely disappeared, a LMCT bands are observed at 544 and 755 nm, which are characteristic changes for the $[Cu^{II}Pc^{3-}]^{1-}$/ $[Cu^{II}Pc^{4-}]^{2-}$reduction (Fig. 7b). Characteristic spectral changes for the Pc based oxidation reaction are observed during

$$[Cl^{1-} - Mn^{III}Pc^{2-}] - e^{-} \overset{E_{1/2}=0.86\ V\ (O(1))}{\Longleftrightarrow} [Cl^{1-} - Mn^{II}Pc^{1-}]^{1+}$$

$$[Cl^{1-} - Mn^{III}Pc^{2-}] + e^{-} \overset{E_{1/2}=-0.13\ V\ (R(1))}{\Longleftrightarrow} [Cl^{1-} - Mn^{II}Pc^{2-}]^{1-}$$

$$[Cl^{1-} - Mn^{II}Pc^{2-}]^{1-} + e^{-} \overset{E_{1/2}=-0.75\ V\ (R(2))}{\Longleftrightarrow} [Cl^{1-} - Mn^{I}Pc^{2-}]^{2-}$$

$$[Cl^{1-} - Mn^{I}Pc^{2-}]^{2-} \longleftrightarrow [Mn^{I}Pc^{2-}]^{1-} + Cl^{1-}$$

$$[Mn^{I}Pc^{2-}]^{1-} + e^{-} \overset{E_{1/2}=-1.11\ V}{\Longleftrightarrow} [Mn^{I}Pc^{3-}]^{2-}$$

$$[Cl^{1-} - Mn^{I}Pc^{2-}]^{2-} + e^{-} \overset{E_{1/2}=-1.38\ V\ (R(3))}{\Longleftrightarrow} [Cl^{1-}Mn^{I}Pc^{3-}]^{3-}$$

$$[Mn^{I}Pc^{3-}]^{2-} + e^{-} \overset{E_{1/2}=-1.63\ V}{\Longleftrightarrow} [Mn^{I}Pc^{4-}]^{3-}$$

$$[Cl^{1-}Mn^{I}Pc^{3-}]^{3-} + e^{-} \overset{E_{1/2}=-1.91\ V\ (R(4))}{\Longleftrightarrow} [Cl^{1-}Mn^{I}Pc^{4-}]^{4-}$$

Scheme 3. Redox mechanism of ***Pc*-Mn**.

the Ox(1) wave as shown in respectively (Fig. 7c). Chromaticity diagram in Fig. 7d illustrates the color changes from cyan (point □: x=0.283 and y=0.343) to blue (point ○: x=0.288 and y=0.296) and then to purple (point △: x=0.309 and y=0.249) after the reduction's and to light green (point ☆: x=0.322 and y=0.345) after the oxidation process.

Fig. 8 represents in-situ UV-Vis spectral changes of ***Pc*-Co** recorded during the redox reactions in DMSO/TBAP electrolyte. At -0.50 V applied potential, the Q band shifts from 672 to 714 nm and a new characteristic bad is observed at 470 nm (Fig. 8a) [46,55,56]. Especially the bad at 470 nm is a characteristic changes for the formation of Co^{+} based complex, thus the spectral changes in Fig. 8a support the $[Co^{II}Pc^{-2}]/[Co^{I}Pc^{-2}]^{1-}$ reduction allocated for R(1) couple of CoPc. Decreasing of the Q band and observation of a broad band at around 550 nm are due to the $[Co^{I}Pc^{-2}]^{1-}/[Co^{I}Pc^{-3}]^{2-}$ process (Fig. 8b). Due to the oxidation of $[Co^{II}Pc^{-2}]$ to $[Co^{III}Pc^{-2}]^{1+}$, the Q band is shifted from 672 nm to different spectral changes than those of CuPc due to the metal based ch60 nm under 0.50 V and then it decreases in intensity at 1.10 V during the further oxidation of $[Co^{III}Pc^{-2}]^{1+}$ to $[Co^{III}Pc^{-1}]^{2+}$ as shown in Fig. 8c. The cyan color (point □: x=0.283 and y=0.343) turns to colorless and then yellow (point △: x=0.379 and y=0.365) after the reduction reactions. Negligible color changes could be observed due to the slight changes in the spectra as shown in Fig. 8d.

More distinct spectral changes are observed during the reduction of ***Pc*-Mn** due to two metal and two Pc based reductions of the complex as shown in Fig. 9. Under open circuit potential the band at 513 nm is characteristic for the Mn^{3+} oxidation state of the MnPc. Moreover, a bathochromic shift on the Q band (751 nm) is observed due to this phenomenon with respect to other complexes [46]. At -0.30 V applied potential, the Q band of the complex disappeared and a new sharp band is recorded at 574 nm. Moreover, the characteristic band of Mn^{3+} at 513 nm is disappeared while new small charge transfer bands are observed at 650, 805, and 853 nm (Fig. 9a,i). Disappearance of the band at 513 nm and the characteristic band of Mn^{2+} at 574 nm indicate the reduction of $[Cl^{1-}\text{-}Mn^{III}Pc^{2-}]$ to $[Cl^{1-}\text{-}Mn^{II}Pc^{2-}]^{1-}$ species during R(1) process. Clear isosbestic points at 451, 661 and 794 nm indicate reversibility of the $[Cl^{1-}\text{-}Mn^{III}Pc^{2-}]$ / $[Cl^{1-}\text{-}Mn^{II}Pc^{2-}]^{1-}$ reduction couple [46,57]. During the R(2) process, the band associated to $[Cl^{1-}\text{-}Mn^{II}Pc^{2-}]^{1-}$ species at 574 nm disappears and a new band at 656 nm increases due to the reduction of $[Cl^{1-}\text{-}Mn^{II}Pc^{2-}]^{1-}$ to $[Cl^{1-}\text{-}Mn^{I}Pc^{2-}]^{2-}$ (Fig. 9a,ii). Spectral changes given in Fig. 9b, are characteristic changes for the further Pc ring reduction processes. During the Ox(1) process, first of all the Q band starts to increase and then all bands decrease in intensity slightly (Fig. 9c). Any change on the position of the Q band illustrate Pc based character of this process. All of these spectral responses support the proposed mechanism given as a result of the voltammetric analysis and in consistence with the literature [44,46,57–59]. As shown in Fig. 9d, distinct color changes are observed during the reduction reactions. Brownish yellow color (point □: x=0.384 and y=0.34387) of the neutral $[Cl^{1-}\text{-}Mn^{III}Pc^{2-}]$ species turn to pink (point ○: x=0.329 and y=0.307), blue (point △: x=0.287 and y=0.278) and then to deep blue (point ⬡: x=0.251 and y=0.213)

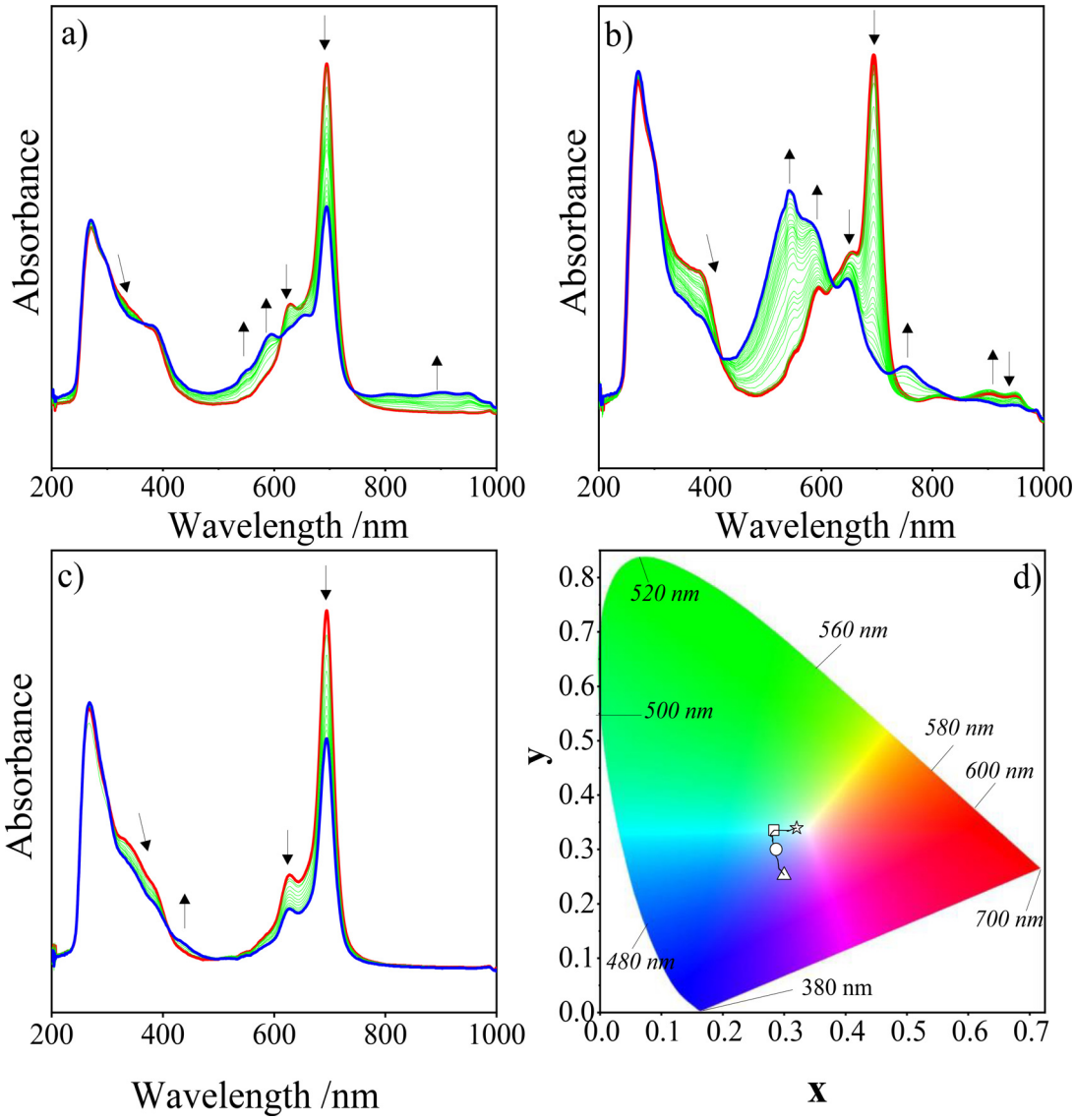

Fig. 7. In-situ UV-Vis spectral changes of ***Pc*-Cu** in DMSO/TBAP electrolyte. **a**) E_{app}= -1.00 V **b**) E_{app}= -1.50 V, **c**) E_{app}= 1.10 V, **d**) Chromaticity diagram (each symbol represents the color of electro-generated species; □: $[Cu^{II}Pc^{-2}]$; ○:$[Cu^{II}Pc^{-3}]^{1-}$; △: $[Cu^{II}Pc^{-4}]^{2-}$; ☆: $[Cu^{II}Pc^{-1}]^{1+}$.

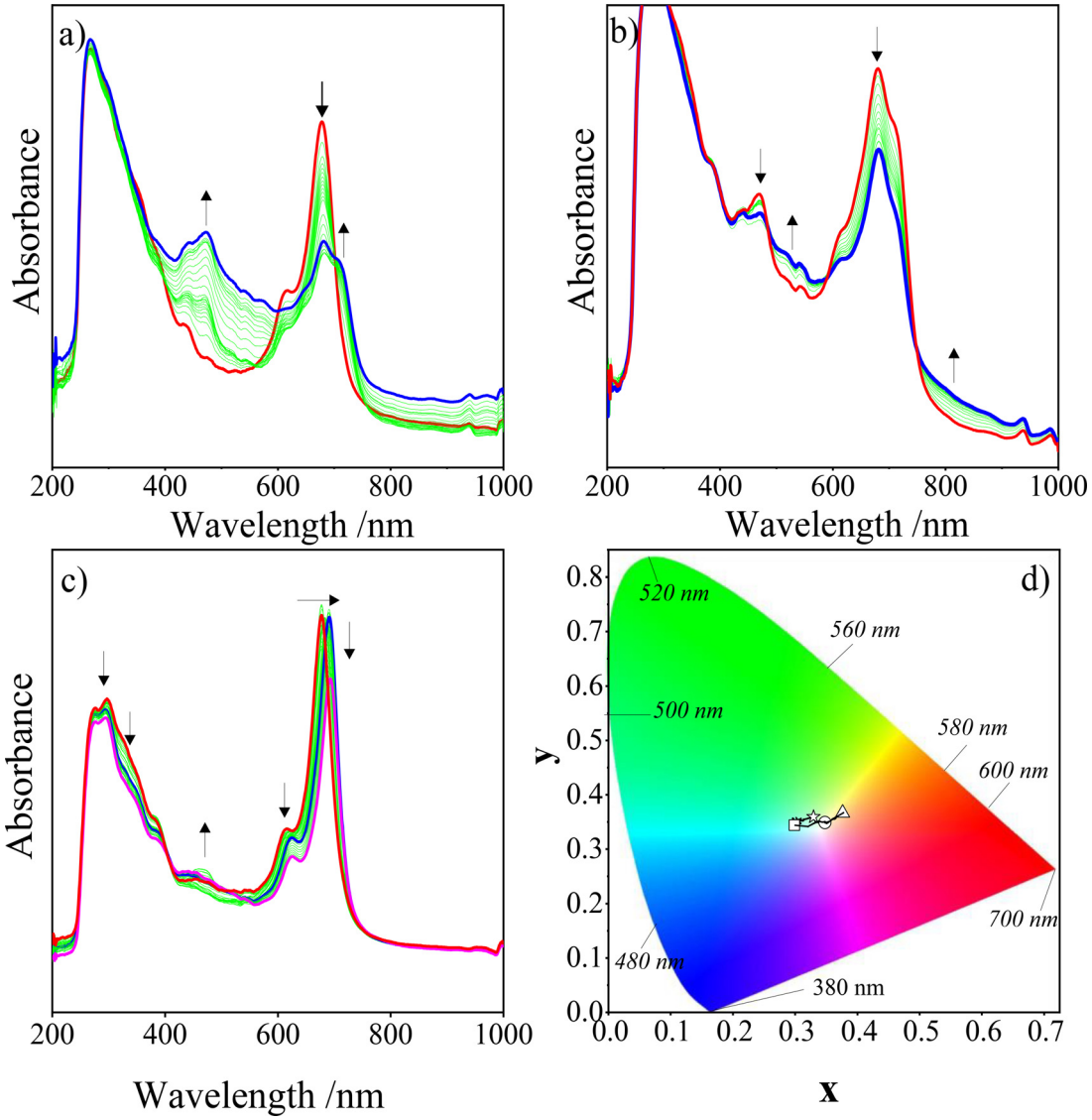

Fig. 8. In-situ UV-Vis spectral changes of CoPc in DMSO/TBAP electrolyte. **a**) E_{app}= -0.50 V **b**) E_{app}= -1.40 V, **c**) E_{app}= 0.50 V and then 1.10 V, **d**) Chromaticity diagram (each symbol represents the color of electro-generated species; □: $[Co^{II}Pc^{-2}]$; ○:$[Co^{I}Pc^{-2}]^{1-}$; △: $[Co^{II}Pc^{-3}]^{2-}$; ☆: $[Co^{III}Pc^{-1}]^{2+}$.

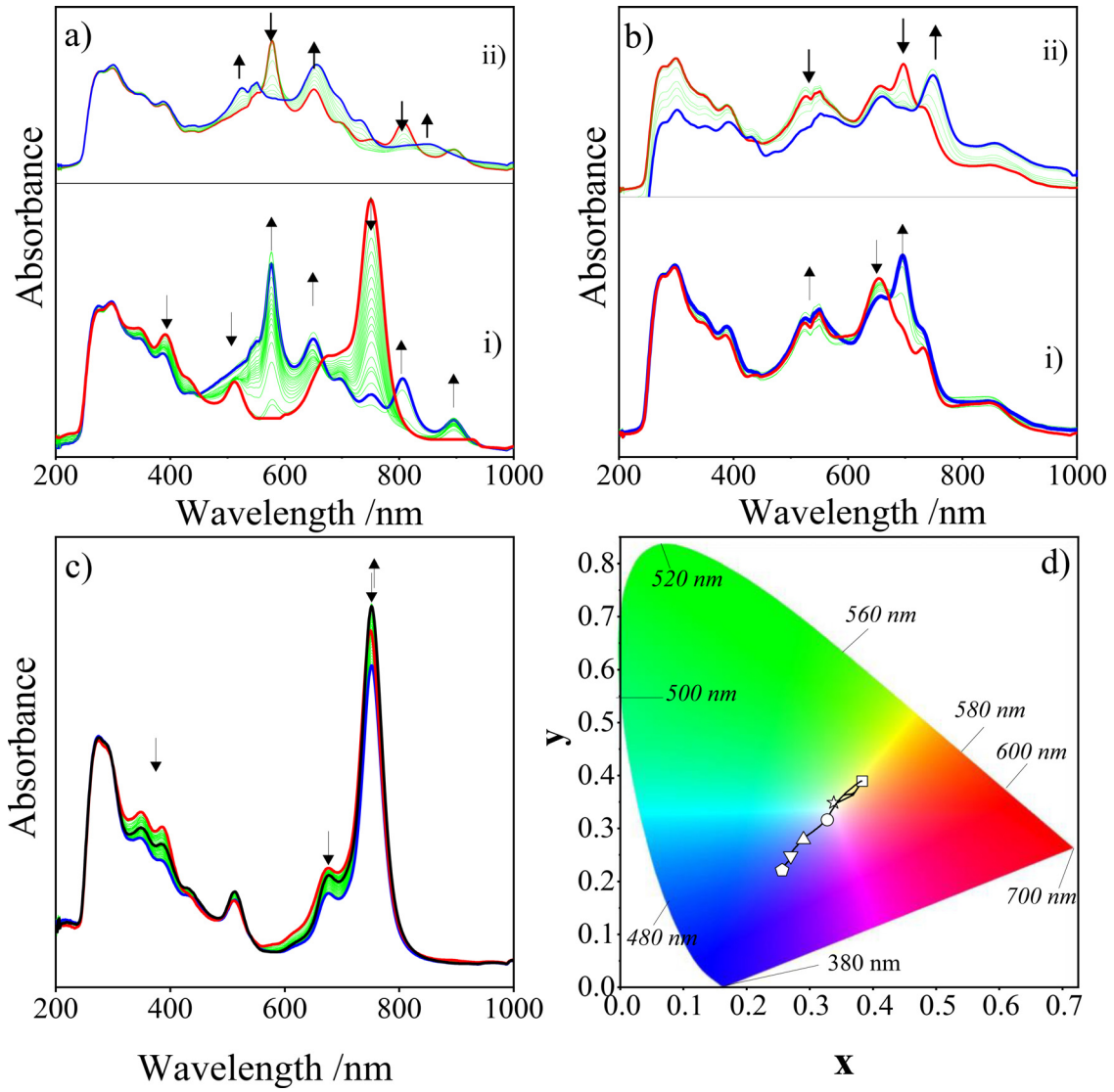

Fig. 9. In-situ UV-Vis spectral changes of MnPc in DMSO/TBAP electrolyte. **a**) i: E_{app}= -0.30 V, ii: E_{app}= -0.90 V **b**) i: E_{app}= -1.50 V and then ii: -2.00 V, **c**) E_{app}= 1.00 V, **d**) Chromaticity diagram (each symbol represents the color of electro-generated species; □: $[Cl^{1-}\text{-}Mn^{III}Pc^{-2}]$; ○:$[Cl^{1-}\text{-}Mn^{II}Pc^{-2}]^{1-}$; △: $[Cl^{1-}\text{-}Mn^{I}Pc^{-2}]^{2-}$; ▽: $[Cl^{1-}\text{-}Mn^{I}Pc^{-3}]^{3-}$; ⬠: $[Cl^{1-}\text{-}Mn^{I}Pc^{-4}]^{4-}$; ☆: $[Cl^{1-}\text{-}Mn^{III}Pc^{-1}]^{1+}$.

after the reduction reactions. After the oxidation reaction, light yellow color (point ☆: x=0.336 and y=0.357) is obtained for the cationic form of the complex. These color differences of the electrogenerated species are fundamental properties for the polyelectrochromic application of the complex.

4. Conclusion

In this study, methoxylated pyrazoline bearing Co^{II} (***Pc*-Co**), Cu^{II} (***Pc*-Cu**) and $Mn^{III}Cl$ (***Pc*-Mn**) phthalocyanines which structures were elucidated by various spectroscopic methods, were synthesized and their electrochemical properties were investigated. Electrochemical behaviors of the MPcs were determined with voltammetric and spectroelectrochemical measurements. Electrochemical responses of the complexes were in consistence with the responses of the similar MPcs. Characteristic Pc based processes of (***Pc*-Cu**) were complicated with the aggregation of the complex. Co^{2+}/Co^{+} reduction and Co^{2+}/Co^{3+} oxidation couples were recorded between the Pc based electron transfer processes due to the location of the d orbitals of Co^{2+} cation between the HOMO and LUMO of Pc ring. Differently two Mn^{3+} based reduction reactions were observed before Pc based ones. Extra metal based redox processes in addition to the Pc based ones enhanced electrochemical worthy of the (***Pc*-Co**) and (***Pc*-Mn**) complexes in various electrochemical application fields. Prominent color changes observed during the redox reactions showd solvotochromic features of the complexes.

Declaration of competing interest

The authors declare that they have no known competing financial interests or personal relationships that could have appeared to influence the work reported in this paper.

Acknowledgements

This work was supported by Office of Scientific Research Projects of Karadeniz Technical University. Project number: FDK-2021-9351. Atıf Koca thanks Turkish Academy of Sciences (TUBA) for support.

Supplementary materials

Supplementary material associated with this article can be found, in the online version, at doi:10.1016/j.jorganchem.2022.122405.

References

[1] M. Ozdemir, G.O. Artuc, E.M. Guler, B. Yalcin, U. Salan, K. Bozali, A.O. Gorgulu, M. Bulut, Dyes and Pigments 196 (2021) 109832.
[2] BS. Erdogan, D. Atilla, A. Gurek, V. Ahsen, Journal of Porphyrins and Phthalocyanines 18 (2014) 139–148.
[3] N. Ndebele, P. Sen, T. Nyokong, Polyhedron 210 (2021) 115518.
[4] G.S. Amitha, S. Vasudevan, Polyhedron 212 (2022) 115591.
[5] P. Sen, J. Mack, T. Nyokong, Journal of Molecular Structure 1250 (2022) 131850.
[6] J. Wang, W. Dong, Z. Si, X. Cui, Q. Duan, Dyes and Pigments 198 (2022) 109985.
[7] Ü. Demirbaş, İ. Ömeroğlu, H.T. Akçay, M. Durmuş, H. Kantekin, Journal of Molecular Structure 1223 (2021) 128992.
[8] A. Alemdar, A.R. Özkaya, M. Bulut, Synthetic Metals 160 (13) (2010) 1556–1565.
[9] N. Kobayashi, W.A. Nevin, Applied Organometallic Chemistry 10 (8) (1996) 579–590.
[10] M. Kaya, E. Menteşe, B. Bilgin Sökmen, H.T. Akçay, Journal of Molecular Structure 1222 (2020) 128870.
[11] H. Yalazan, D. Akyüz, V. Serdaroğlu, N. Kahriman, A. Koca, H. Kantekin, Journal of Organometallic Chemistry 912 (2020) 121181.
[12] H. Yalazan, D. Akyüz, D. Ünlüer, A. Koca, H. Kantekin, K. Sancak, Polyhedron 180 (2020) 114419.
[13] A. Koca, Electrochemistry communications 11 (2009) 838–841.
[14] A. Alsudairi, J. Li, N. Ramaswamy, S. Mukerjee, K. Abraham, Q. Jia, The journal of physical chemistry letters 8 (2017) 2881–2886.
[15] S. Roy, M. Miller, J. Warnan, J.J. Leung, C.D. Sahm, E. Reisner, ACS Catalysis 11 (2021) 1868–1876.
[16] K.I. Ozoemena, T. Nyokong, Electrochim. Acta 51 (2006) 5131–5136.
[17] V. Mani, R. Devasenathipathy, S.-M. Chen, S.-T. Huang, V. Vasantha, Enzyme Microb. Technol. 66 (2014) 60–66.
[18] D. Akyüz, A. Koca, Sensors and Actuators B: Chemical 283 (2019) 848–856.
[19] O. Koyun, S. Gorduk, M. Gencten, Y. Sahin, New Journal of Chemistry 43 (2019) 85–92.
[20] H. Xu, J. Xiao, B. Liu, S. Griveau, F. Bedioui, Biosensors and Bioelectronics 66 (2015) 438–444.
[21] M.K.S. Monteiro, S.S.M. Paiva, D.R. da Silva, V.J.P. Vilar, C.A. Martínez-Huitle, E.V. dos Santos, Journal of Electroanalytical Chemistry 839 (2019) 283–289.
[22] C.-L. Lin, C.-C. Lee, K.-C. Ho, J. Electroanal. Chem. 524 (2002) 81–89.
[23] C. Solis, E. Baigorria, M.E. Milanesio, G. Morales, E.N. Durantini, L. Otero, M. Gervaldo, Electrochim. Acta 213 (2016) 594–605.
[24] C. Hunt, M. Mattejat, C. Anderson, L. Sepunaru, G. Ménard, ACS Applied Energy Materials 2 (2019) 5391–5396.
[25] K.P. Madhuri, N.S. John, Appl. Surf. Sci. 449 (2018) 528–536.
[26] H. Karaca, J. Organomet. Chem. 822 (2016) 39–45.
[27] C.G. Claessens, U. Hahn, T. Torres, Phthalocyanines: From outstanding electronic properties to emerging applications, The Chemical Record 8 (2008) 75–97.
[28] A. Günsel, A.T. Bilgiçli, M. Kandaz, E.B. Orman, A.R. Özkaya, Dyes and Pigments 102 (2014) 169–179.
[29] V. Mani, R. Devasenathipathy, S.-M. Chen, J.-A. Gu, S.-T. Huang, Renewable Energy 74 (2015) 867–874.
[30] A. Kumar, V.K. Vashistha, D.K. Das, Coord. Chem. Rev. (2020) 213678.
[31] R. Li, X. Zhang, P. Zhu, D.K. Ng, N. Kobayashi, J. Jiang, Inorganic chemistry 45 (2006) 2327–2334.
[32] R. Bayrak, S.K. Ataşen, I. Yılmaz, İ. Yalçın, M. Erman, Y. Ünver, İ. Değirmencioğlu, Journal of Molecular Structure 1231 (2021) 129677.
[33] L-L. Tong, Y. He, L-N. Niu, L-L. Bao, Z-C. Wei, Y. Liao, C-B. Guo, Synthetic Metals 210 (2015) 133–140.
[34] S.S. Pathade, V.A. Adole, B.S. Jagdale, Current Research in Green and Sustainable Chemistry 4 (2021) 100172.
[35] A. Nas, Z. Biyiklioglu, S. Fandaklı, G. Sarkı, H. Yalazan, H. Kantekin, Inorganica Chimica Acta 466 (2017) 86–92.
[36] S. Altun, Z. Odabaş, A. Altındal, A.R. Özkaya, Dalton Trans 43 (2014) 7987–7997.
[37] M.J. Stillmann, T. Nyokong in: C.C. Leznoff, A.B.P. Lever, in: Phthalocyanines: Properties and Applications, VCH, New York, USA, 1989, pp. 133–257.
[38] D. Çakır, O. Bekircan, Z. Biyiklioglu, Synthetic Metals 201 (2015) 18–24.
[39] B. Ertem, G. Sarkı, H. Yalazan, Z. Bıyıklıoğlu, H. Kantekin, Inorganica Chimica Acta 462 (2017) 123–129.
[40] A. Günsel, A.T. Bilgiçli, M. Kandaz, E.B. Orman, A.R. Özkaya, Dyes Pigm 102 (2014) 169–179.
[41] J. Obirai, T. Nyokong, Electrochimica acta 50 (2005) 3296–3304.
[42] G. Mbambisa, P. Tau, E. Antunes, T. Nyokong, Polyhedron 26 (2007) 5355–5364.
[43] A. Koca, A.R. Özkaya, M. Selçukoğlu, E. Hamuryudan, Electrochimica acta 52 (2007) 2683–2690.
[44] J. Obirai, N.P. Rodrigues, F. Bedioui, T. Nyokong, Journal of Porphyrins and Phthalocyanines 7 (2003) 508–520.
[45] M. L'HER, A. PONDAVEN, Electrochemistry of 104, The Porphyrin Handbook (2003) 117.
[46] A. Koca, Spectroelectrochemistry of phthalocyanines, in: Electrochemistry of N4 Macrocyclic Metal Complexes, Springer, 2016, pp. 135-200.
[47] A. Lever, P. Minor, J. Wilshire, Inorganic Chemistry 20 (1981) 2550–2553.
[48] A. Lever, P. Minor, Electrochemistry of main-group phthalocyanines, Inorganic Chemistry 20 (1981) 4015–4017.
[49] N. Sehlotho, M. Durmuş, V. Ahsen, T. Nyokong, Inorg. Chem. Commun. 11 (2008) 479–483.
[50] B. Agboola, K.I. Ozoemena, P. Westbroek, T. Nyokong, Electrochimica acta 52 (2007) 2520–2526.
[51] S. Arslan, I. Yilmaz, Inorganic Chemistry Communications 10 (2007) 385–388.
[52] E.T. Saka, G. Sarkı, H. Kantekin, A. Koca, Synthetic Metals 214 (2016) 82–91.
[53] M. Arıcı, D. Arıcan, A.L. Uğur, A. Erdoğmuş, A. Koca, Electrochim. Acta 87 (2013) 554–566.
[54] Z.P. Ou, Z. Jiang, N.S. Chen, J.L. Huang, J. Shen, K.M. Kadish, J. Porphyrins Phthalocyanines 12 (2008) 1123–1133.
[55] W. Nevin, W. Liu, M. Melnik, A. Lever, Journal of electroanalytical chemistry and interfacial electrochemistry 213 (1986) 217–234.
[56] A. Alemdar, A.R. Özkaya, M. Bulut, Polyhedron 28 (2009) 3788–3796.
[57] D. Quinton, E. Antunes, S. Griveau, T. Nyokong, F. Bedioui, Inorganic Chemistry Communications 14 (2011) 330–332.
[58] A.M. Sevim, H.Y. Yenilmez, M. Aydemir, A. Koca, Z.A. Bayır, Electrochim. Acta 137 (2014) 602–615.
[59] İ. Özçeşmeci, A. Koca, A. Gül, Electrochim. Acta 56 (2011) 5102–5114.
[60] D. Akyüz, T. Keleş, Z. Biyiklioglu, A. Koca, J. Electroanal. Chem. 804 (2017) 53–63.
[61] A.A. Esenpınar, A.R. Özkaya, M. Bulut, Journal of Organometallic Chemistry 696 (2011) 3873–3881.
[62] J. Obirai, T. Nyokong, Electrochimica Acta 50 (2005) 3296–3304.
[63] Ü.E. Özen, T. Keleş, Z. Bıyıklıoğlu, A. Koca, A.R. Özkaya, Journal of The Electrochemical Society 163 (2016) B673–B682.